IL NUOVO CIMENTO Vol. 31 C, N. 5-6 Settembre-Dicembre 2008
DOI 10.1393/ncc/i2009-10358-y

The structure of turbulent jets, vortices and boundary layer: Laboratory and field observations

E. Sekula(*) and J. M. Redondo(**)

Departamento de Fisica Aplicada, Universitat Politecnica de Catalunya, Campus Nord Edifici B4/B5, C/ Jordi Girona Salgado, 1-3, 08034 Barcelona, Spain

(ricevuto il 25 Dicembre 2008; approvato il 30 Marzo 2009; pubblicato online il 22 Luglio 2009)

Summary. — The main aim of this work is research, understand and describe key aspects of the turbulent jets and effects connected with them such as boundary layer interactions or the effect of a 2D geometry. Work is based principally on experiments but there are also some comparisons between experimental and field results. A series of experiments have been performed consisting in detailed turbulent measurements of the 3 velocity components to understand the processes of interaction that lead to mixing and mass transport between boundaries and free shear layers. The turbulent wall jet configuration occurs often in environmental and industrial processes, but here we apply the laboratory experiments as a tool to understand jet/boundary interactions in the environment. We compare the structure of SAR (Synthetic Aperture Radar) images of coastal jets and vortices and experimental jets (plumes) images searching for the relationship between these two kinds of jets at very different Reynolds numbers taking advantage of the self-similarity of the processes. In order to investigate the structure of ocean surface detected jets (SAR) and vortices near the coast, we compare wall and boundary effects on the structure of turbulent jets (3D and 2D) which are non-homogeneous, developing multifractal and spectral techniques useful for environmental monitoring in space.

PACS 47.60.Kz – Flows and jets through nozzles.
PACS 92.10.Lq – Turbulence, diffusion, and mixing processes in oceanography.
PACS 94.05.Lk – Turbulence.

1. – Introduction

Turbulence is a phenomenon that can be found anywhere, at every turn of life, from the stirring of a coffee cup to the wind in the atmosphere or the solar wind. Most

(*) E-mail: emil.sekula@gmail.com
(**) E-mail: redondo@fa.upc.edu

flows occurring in nature and in engineering applications are turbulent. There is a lot of interest in the boundary layers because most of the transport is actually regulated by the regions that constrain or act as transport barriers, many laboratory techniques in image analysis and data processing may also be used in real environmental flows, but we have to find more precise methods to calculate properties of the boundary layer. Amid many parameters such as the displacement thickness, the skin-friction coefficient, it is helpful to uncover the prediction of mean velocity and shear-stress distribution across the layer. There is also continuing research interest aimed toward finding an understanding of turbulent shear flows of which the boundary layer is probably the most interesting example. In this context the use of structure function and fractal methods are useful to investigate the turbulent cascade structures. Experimental and geophysical observations are investigated with multi-scale techniques in order to extract relevant information on the spectral characteristics of mixing and diffusive events. Both density and tracer marked interfaces are investigated in several experimental configurations where different tracers are diffused by means of unstable jets [1]. Both plane and vertical configurations are used, where the initial density difference is characterized by the Atwood number. The evolutions of the jets reach maximum complexity and local mixing efficiency when there are interactions with walls and boundary layers. The diffusion and structure of jets and vortices in the ocean are also investigated using multifractal techniques [2], mixing parameters [3], ESS and structure functions, that indicate strong inverse cascades towards the large scales producing spectral variations [4].

The intermittency is obtained by relating it to the sixth- and third-order structure function scaling exponents and to the measurements of maximum fractal dimension of scalars (dye) advected in the flow. Several uses of this new technique are proposed [5]. We use the laboratory experimental results to maximize the additional spectral and multifractal information from remote-sensing SAR images so that different areas dominated by buoyancy, momentum or vorticity cascades may be identified. First we present the basic average (mean and fluctuating) equations that describe the flows used in the laboratory experiments for wall jets. In sect. **3** we describe the experiments and in sect. **4** the experimental results. In sect. **5** we present the image analysis of river-induced jets in the ocean as well as in the laboratory. We finally discuss the laboratory and remote-sensing analysis presenting the conclusions.

2. – Basic equations for turbulent jets and plumes

Across the boundary layer the flow velocity changes from zero at the boundary to some finite value characteristic of an inviscid fluid not affected by the friction. The equation of motion in the x-direction becomes

$$\frac{\partial u}{\partial t} + u\frac{\partial u}{\partial x} + v\frac{\partial u}{\partial y} = -\frac{1}{\rho}\frac{\partial p}{\partial x} + v\frac{\partial^2 u}{\partial y^2}\,. \tag{1}$$

The velocity component v normal to the boundary must also be small, and the

mass-conservation equation is

$$(2)\qquad \begin{cases} \dfrac{\partial u'}{\partial t'} + u'\dfrac{\partial u'}{\partial x'} + v'\dfrac{\partial u'}{\partial y'} = -\dfrac{\partial p'}{\partial x'} + \dfrac{1}{R}\dfrac{\partial^2 u'}{\partial x'^2} + \dfrac{\partial^2 u'}{\partial y'^2}\,, \\ \dfrac{1}{R}\left(\dfrac{\partial v'}{\partial t'} + u'\dfrac{\partial v'}{\partial x'} + v'\dfrac{\partial v'}{\partial y'}\right) = -\dfrac{\partial p'}{\partial y'} + \dfrac{1}{R^2}\dfrac{\partial^2 v'}{\partial x'^2} + \dfrac{1}{R}\dfrac{\partial^2 v'}{\partial y'^2}\,, \\ \dfrac{\partial u'}{\partial x'} + \dfrac{\partial v'}{\partial y'} = 0, \end{cases}$$

$$\text{where} \begin{cases} x' = \dfrac{x}{L}, \quad y' = R^{1/2}\dfrac{y}{L}\,, \quad t' = \dfrac{tU_0}{L}\,, \\ u' = \dfrac{u}{U_0}, \quad v' = R^{1/2}\dfrac{v}{U_0}, \quad p' = \dfrac{p - p_0}{\rho U_0^2}, \end{cases}$$

being: R—Reynolds number, L—dissipation scale, U_0—mean velocity and p_0—uniform pressure.

Aside from the usual consideration for technological applications, the turbulent boundary layer is worth studying because it is especially rich in details and complications, although it is a simple, well-defined flow. As the flow is bounded by one solid boundary and by one free boundary, it exhibits the details one normally associates with confined flows, termed "wall turbulence". In these respects it is similar to channel and pipe flow. On the other hand, near to the free boundary it incorporates also the features of "free turbulence" found in wakes and jets. This combination brings us to the most fascinating question, namely exactly how the two different types of flow match with each other.

Many of the ideas originated essentially with Prandtl and were based on the use of the turbulent energy equation:

$$(3)\qquad \frac{1}{2}\left(\overline{U}\frac{\partial \overline{q}^2}{\partial x} + \overline{V}\frac{\partial \overline{q}^2}{\partial y}\right) = -\overline{uv}\frac{\partial \overline{U}}{\partial y} - \frac{\partial}{\partial y}\left[\overline{v\left(\frac{p}{\rho}\right) + \frac{q^2}{2}}\right] - \varepsilon,$$

where $\overline{U}$ and $\overline{V}$ are the streamwise and normal components of the mean velocity, u and v are the corresponding fluctuations, q is the absolute magnitude of the velocity fluctuation vector: $q^2 = u_i u_i$, p is the pressure, and ε is the viscous energy dissipation per unit volume.

Turbulent jets are fluid flows produced by a pressure drop through an orifice. Their mechanics, although studied for over fifty years, has recently received research attention that has resulted in a much-improved understanding of the process by which they entrain surrounding fluids. Turbulent plumes are fluid motions whose primary source of kinetic energy and momentum flux is body forces derived from density inhomogeneities. Plumes have not been studied in the same detail as jets but nevertheless there have been some recent gains in the understanding of their behaviour.

If, for example, a jet of water coming from a plane nozzle of large length into a large body of water or a jet of air into a large expanse of air, we use suitable flow visualisation techniques, we will find that the jet mixes violently with the surrounding fluid creating turbulence and the jet itself grows thicker. Experimental observations on the mean turbulent velocity field indicate that in the axial direction of the jet, one could divide the

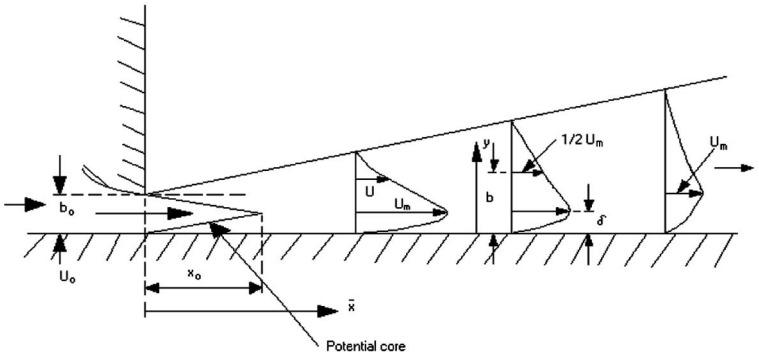

Fig. 1. – Sketch of a plane turbulent wall jet.

jet flow into two distinct regions. In the first region, close to the nozzle, known commonly as the flow development region, as the turbulence penetrates inwards towards the axis or centreline of the jet, there is a wedge-like region of undiminished mean velocity, equal to U_0. This wedge is known as the potential core and is surrounded by a mixing layer on top and bottom. In the second region, known as the fully developed flow region, the turbulence has penetrated to the axis and as a result, the potential core has disappeared.

In the fully developed flow region, the transverse distribution of the mean velocity in the x-direction, *i.e.* the variation of u with y at different sections, has the same geometrical shape.

At every section, u decreases continuously from a maximum value of u_m on the axis to a zero value at some distance from the axis. The free jets have top-hat velocity distributions in the potential core.

Because a free jet entrains fluid from both sides, it spreads faster, and, therefore, its centreline velocity decays faster than that of a wall jet. We present next equations of motion (4), (5) and integral momentum equation (6) or (7) for the wall jet case:

$$u\frac{\partial u}{\partial x} + v\frac{\partial u}{\partial y} = -\frac{1}{\rho}\frac{\mathrm{d}p}{\mathrm{d}x} + v\frac{\partial^2 u}{\partial y^2} + \frac{1}{\rho}\frac{\partial \tau_t}{\partial y}\,, \tag{4}$$

$$\frac{\partial u}{\partial x} + \frac{\partial v}{\partial y} = 0, \tag{5}$$

$$\frac{\mathrm{d}}{\mathrm{d}x}\int_0^\infty \rho u^2 \mathrm{d}y = 0 \ \ (\text{if } \tau_0 \text{ is neglected}), \tag{6}$$

where τ_0 is the wall shear stress.

We can rewrite (6) as

$$\frac{\mathrm{d}}{\mathrm{d}x}\rho u_m^2 b\int_0^\infty f^2 \mathrm{d}\eta = 0, \tag{7}$$

being: τ_t—turbulent shear stress, b—distance between the wall and point where $u = 1/2\,u_m$ (see fig. 1), u_m—maximum velocity, f—function guessed on the basis of available experiments.

Wall jets are of great and diverse engineering importance and engineering applications often feature 2D or 3D wall jets.

Wall laws derived from experiments in the similarity region are thus used to complete the solution of the problem, which implies that such a numerical resolution is possible only if experiments are available for the studied configuration. Elevating an axisymmetric jet from a wall and adding a back plane is complex due to the numerous interactions that determine the behaviour of the flow. This situation seems to be most common in practical jet applications [6, 7].

Because most practical applications involve the near field of wall jets, it is important to study the distribution of velocities and turbulent stresses in these regions. Let us consider a plane jet of thickness b_0 and uniform velocity U_0 coming out of a nozzle tangentially to a smooth flat plate which is submerged in a semi-finite expanse of the same fluid as shown in fig. 1.

The resulting flow can be viewed as a combination of an inner wall boundary layer, where the velocity increases from zero at the wall to a local maximum, and an outer free jet where the flow decreases from a local maximum to zero (or the free stream value in the case of moving surroundings). The strong interaction between these two layers causes the complexity of this type of flow. Evidence for this interaction is the low spreading rate (less than for the corresponding free jet) and the influence on the flow near the wall is shown by the displacement of the position of zero shear stress away from the point of maximum mean velocity. As the jet leaves the nozzle, due to the velocity discontinuity, a shear layer develops on the fluid side. A boundary layer develops on the wall side. When the boundary layer meets the penetrating shear layer, the potential core of the jet is consumed and beyond this section, the flow is said to be fully developed.

If we make experimental observations of the distribution of the u-velocity in the y-direction at different x-stations, that is, if we study the $u(y)$ function for various values of x, we find that the shape of the velocity profile is the same at all x-stations in the fully developed flow region. We find that at any x-station, u increases from zero at the wall to a maximum value of u_m at $y = \delta$ and then decreases to zero at some large value of y. The region from the wall to the maximum velocity level is known as the boundary layer and the region above this is generally known as the free mixing region. The velocity scale is generally represented by u_m and the length scale b is taken as the value of y where $u = 1/2u_m$ and $\partial u/\partial y$ is negative.

It is interesting to find that the velocity profiles are indeed similar. The phenomenon described above is known as the plane turbulent wall jet with differential and integral equations (8), (9) that may be written as

$$g' = \frac{bu'_m}{u_m}\left(f^2 - f'\int_0^\eta f\mathrm{d}\eta\right) - b'(\eta f f' - f') - \frac{\nu}{u_m b}f'', \tag{8}$$

where $g' = \mathrm{d}g/\mathrm{d}\eta$, $f' = \mathrm{d}f/\mathrm{d}\eta$ and $f'' = \mathrm{d}^2 f/\mathrm{d}\eta^2$

$$2\frac{\mathrm{d}}{\mathrm{d}x}\rho {u_m}^2 b\int_0^\infty f^2\mathrm{d}\eta \propto x^S. \tag{9}$$

Using on the same experiments more than one method of diagnostic allows us to compare results and improve the understanding of the flows and of the laboratory techniques, this is also an important argument for network-based research because the new experimental techniques implemented (*e.g.*, LIF, PIV, particle tracking, fractal analysis, intermittency, structure function analysis, etc.) may be useful to other researchers in experimental fluid dynamics or in related fields.

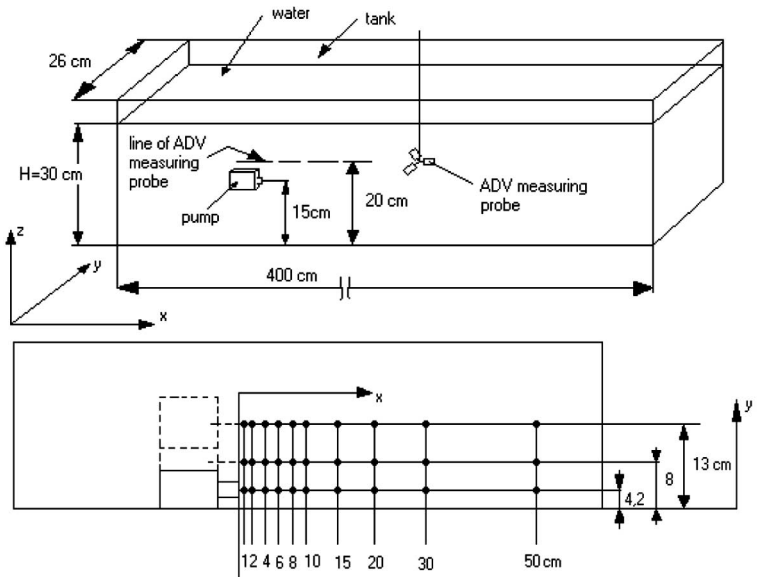

Fig. 2. – Experimental set-up (top) and positions of the measuring points at the wall jet centreline (below).

Different experiments have been previously done with turbulent jets. We present here measurements on the turbulent structure of wall jet flows including spectral measurements of the non-homogeneous turbulent cascade processes and thus complement previous experiments, which were mostly concerned with mean structure. Hinze [8] described transport processes in turbulent flows, free turbulent shear flows and "wall" turbulent shear flows. A basic description of turbulent jets cited in Rajaratnam [9] or the scaling differences between plane jets and measurements in radial wall jets are discussed by Knowles *et al.* [10] confirming axisymmetry in round, turbulent jets impinging normally on a flat plate and self-similarity in the velocity profiles. Similar research works cited in the *Annual Review of Fluid Mechanics* [6, 7] discuss engineering details and particular cases.

There are many other research works and results describing different aspects of wall jet flows, but they in majority use a fundamental Kolmogorov theory. Considering the new advances in non-homogeneous turbulent structure [1, 11] we show new measurements that will help to understand the role of turbulent cascades when affected by coherent structures.

3. – Laboratory experiments, data analysis and set-up

We study here the turbulent jets and effects connected with them, which are similar in experimental and environmental fields. A series of experiments have been performed consisting on detailed turbulent measurements of the 3 components of velocity to obtain a basic understanding on the processes of interaction that lead to mixing and mass transport between boundaries and free shear layers. The used configurations are explained providing information about the characteristics of the turbulent free jet, the circular jet and the turbulent wall jet. Comparisons between different experiments with the above configurations provide information on the entrainment and mixing properties thanks to the study of structure functions. Measurements of turbulent jets [12] and of their

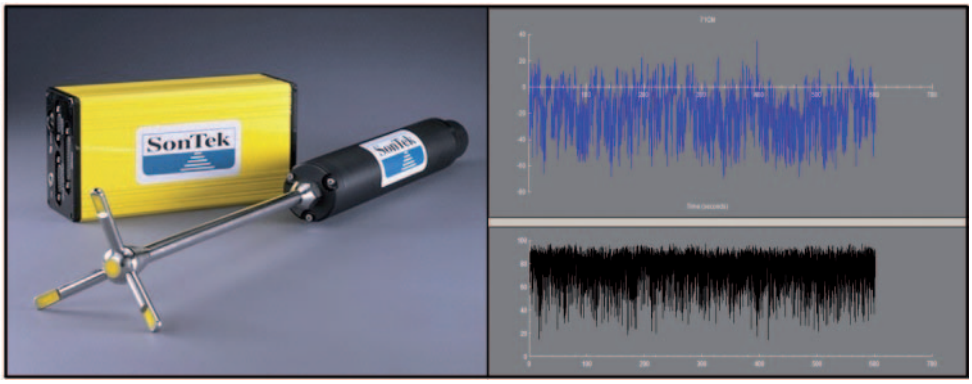

Fig. 3. – Acoustic Doppler Velocimeter (left) and time series of x-component (right, top) and their average correlation score, which is used for data quality.

self-similar image analysis [13] have been very useful to understand the scaling structure of these flows. Figure 2 shows experimental set-up and some positions of the measuring points with coordinate system marked and position of jets'source (pump) and ADW measuring probe. Geometrical dimensions are presented too.

The SonTek ADV (Acoustic Doppler Velocimeter) is a versatile, high-precision instrument used to measure 3-axis (3D) water velocity (fig. 3). The ADV is used to measure water velocity in a wide range of environments including laboratories, rivers, estuaries, and the ocean. ADV performance has been shown to compare favorably with laser Doppler systems costing ten times as much. In addition, the ADV is extremely simple to set up and use. Evaluation of the Acoustic Doppler Velocimeter for Turbulence Measurements is presented by Voulgaris *et al.* [14].

The ADV uses acoustic Doppler technology to measure 3D flow in a small sampling volume located a fixed distance (5 or 10 cm) from the probe. Some basic parameters of ADV used in the experiments were: a sampling rate of 25 Hz, a sampling volume: 0.25 cm^3, high accuracy of less than 1% of measured range and a wide velocity range between 1 mm/s and 2.5 m/s.

The 3 components of the turbulent velocity were measured downstream at the jet nozzle up to $x/D = 110$ for a wall jet centreline placed at 4 cm, 8 cm and 13 from the side wall of the 4 m tank.

4. – Results of the laboratory experiments

Spectral distribution of energy is one of the methods providing first, basic information of turbulent flows. We present here (fig. 4) one example of the energy spectrum for a downstream distance $x/D = 65$ of the "wall" jet case ($y = 4$ cm) in order to show the scale-to-scale energy transfer that depends on the local processes occurring downstream of the wall jet, thus an analysis of the different positions is needed.

Different slopes of power spectrum for variable frequency range show distinct scale processes depending on the jet zone.

Some basics results (such as velocity components, turbulent kinetic energy, Signal-To-Noise Ratio (SNR) and average correlation) calculated with ADV software (WinADV) are shown in fig. 5.

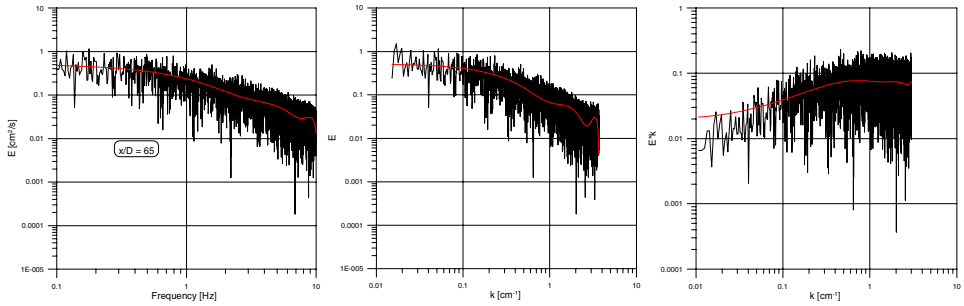

Fig. 4. – Different power spectrum configurations for $x/D = 65$ (normal jet case, $y = 4\,\mathrm{cm}$).

We can observe a velocity reduction in initial jet's zone ($x/D < 20$). There are demonstrated measurement difficulties in this region due to the nozzle proximity and potential core existence. This effect is not so visible for y velocity component. Respectively the turbulent kinetic energy draws an analogy. SNR is the ratio of signal strength to the background acoustic noise level inherent in the ADV instrument. The values are given in dB relative to the noise level.

For the instantaneous velocity data a signal-to-noise ratio of 15 dB or higher should be maintained. For measuring mean velocities, the signal-to-noise ratio should be 5 dB or higher. Our data comply with these conditions.

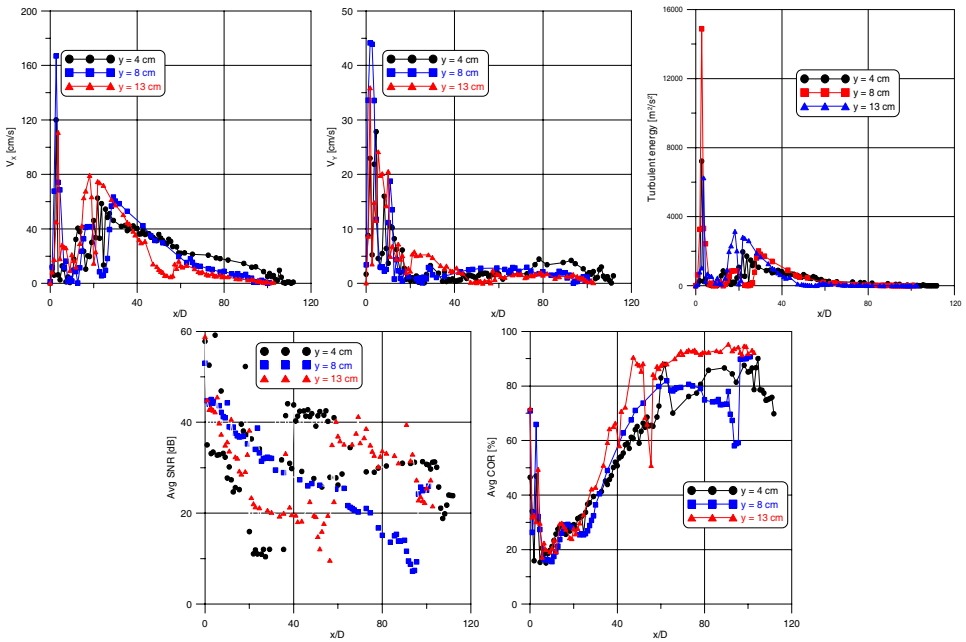

Fig. 5. – Two velocity components, turbulent kinetic energy, Signal-To-Noise Ratio (SNR) and average correlation for the normal jet case and $y = 4\,\mathrm{cm}$.

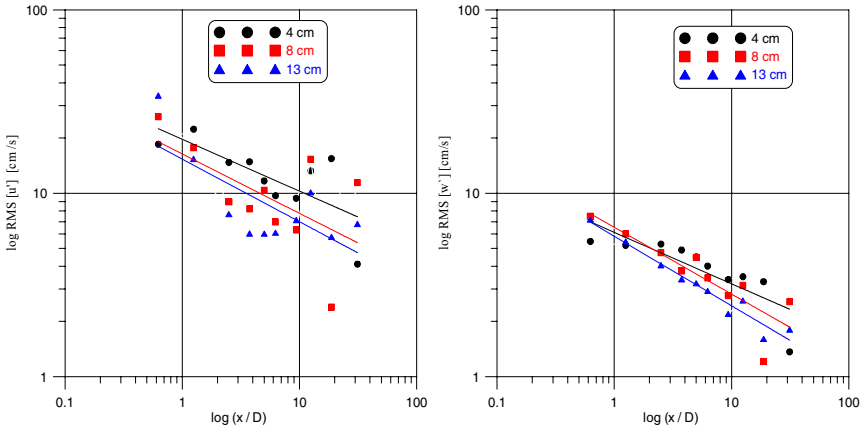

Fig. 6. – Decay of the jet centreline RMS turbulent velocity for x (left) and z (right) components at different distances from the wall for low Reynolds number case.

A correlation score is calculated for each sample stored in the ADV file, for each of the three signal beams; values are expressed in percent, with 100 being a perfect correlation. Correlations of 70 to 100 percent are typically considered good. Low correlation values may indicate problems related to turbulence, signal strength, scatterer density, excessive air bubbles, or problems with the probe itself. For smaller x/D values we do not have sufficient correlation score because there is not enough precision for 25 Hz and the turbulence is not fully developed.

Comparison of the standard deviation for two turbulent (regarding the jet development) velocity components ($V_X = u'$ and $V_Z = w'$) shows the much more important role of the wall boundary layer on the V_X component (see fig. 6). The greatest interaction occurs at x/D between 10 and 30 for the low Reynolds number wall jet. A significant increase in u' (left) is observed due to the wall-induced vorticity, it is obvious that it will affect more the u' than the w' components.

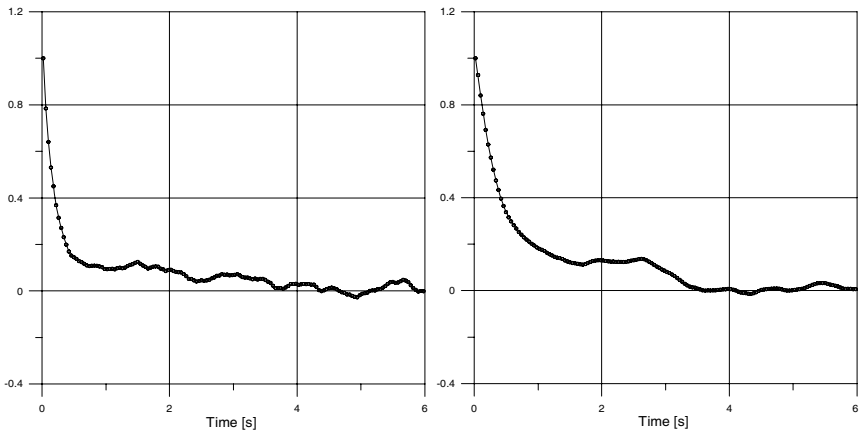

Fig. 7. – Correlation function for two measurement points (normal jet case, $y = 4$ cm): $x/D = 55$ (left) and $x/D = 76$ (right).

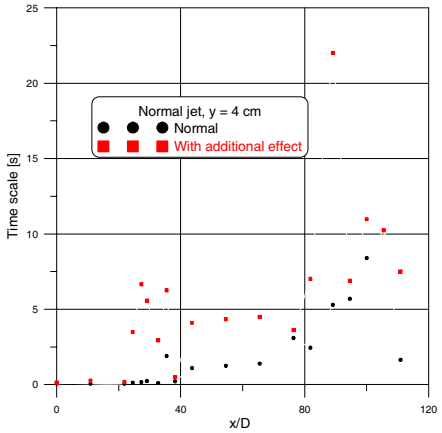

Fig. 8. – Increase of the integral time scale with downstream distance is perceptible. Squares correspond to time scales that seem to be a combination of two or more effects, such as the correlation plot shown in fig. 7 (right).

One of the permanent problems of turbulence analysis is to find appropriate length and time scales. One of the methods to define them is using correlation functions. The form of correlation function depends on the character of turbulence. In fig. 7 we show two examples of the normalized time correlation for the longitudinal velocity component at the jet centreline. The two examples have been chosen to have a similar integral time scale of about 3 seconds, but at $x/D = 76$, two dominant scales seem to be interacting and produce the hump detected at 2–3 s (called here "additional effect"). Figure 8 shows two case time scales in downstream distance for normal jet case and wall jet configuration. Higher values of "additional effect" time scales are observable.

One of the characteristics of the experiment was to measure at each point during a long time, assuring the stationarity of the turbulence, the main reason was to be able to calculate with the minimum error structure functions of the highest possible order.

The velocity structure functions of order p are defined in terms of the moments of velocity differences as

$$S_P(l) = \left\langle \left(u\left(\vec{x} + \vec{l}\right) - u(\vec{x}) \right)^P \right\rangle = \left\langle (\delta u_l)^P \right\rangle, \tag{10}$$

where $\langle \ldots \rangle$ indicates ensemble average and u is the velocity component parallel to $\vec{l}$.

Especially the third-order structure function of the velocity is important in our analysis of intermittency and scale-to-scale and multifractal characteristics. It is proportional to the separation distance l in the inertial range of energy spectra and it is standard procedure in the analysis to define an inertial range. But this is predicted by Kolmogorov's theory (1941) and in non-homogenous and non-isotropic turbulence this proportionality is not warranted. That is why is so interesting to compare third-order structure function but also absolute scaling exponent, relative scaling exponent and the intermittency parameter. Detailed information about this problem is presented in Mahjoub [11, 15], higher-order structure functions are difficult to calculate as the error grows with the order [13]. We will just present some relationships between the spectral exponents, which are of course related to the second-order structure functions.

5. – Image analysis of experimental jets (plumes) and the sea surface

We also use the multifractal analysis of SAR and experimental jets (plumes) images looking for relationship between these two kinds of jets with respect to multifractal dimension analysis.

The SAR images exhibit a large variation of natural features produced by winds, internal waves, the bathymetric distribution, by thermal or solutal convection by rain, etc. These produce variations in the sea surface roughness.

The satellite-borne SAR is able to detect oceanic features with a range of scales as seen in fig. 7, which shows several jet-like structures in the Gulf of Lion area. The spatial cross-correlation may give an indication of the length over which such features are correlated. Let $\rho(x)$ be the intensity of the SAR backscatter at point x and $\rho(x+\lambda)$ the intensity at a point separated a distance λ from the first one. The normalised average

$$R(\lambda) = \frac{\langle \rho(x)\rho(x+\lambda)\rangle}{\langle \rho(x)^2\rangle} \tag{11}$$

defines the normalized cross-correlation of $\rho(x)$ over the area where the average is taken.

The integral length scale associated to the sea surface roughness correlation obtained integrating (11) indicates the spatial scale l where the SAR intensities are well correlated. If we suppose that the surface currents are responsible (at least partly) for the spatial distribution of the ocean roughness, the slope at both sides of an eddy is very different at producing radar backscatter from a side (as happens with ERS-1/2 and also ENVISAT). Other reason is that the surface tensioactivity (natural or man produced) will be advected by the current lines relating the scalar and the vorticity distribution within the complex mesoscale ocean surface topology. It is interesting to compare the multifractal appearance of the different signatures (for example jets) and this is shown in fig. 9.

Differences in the multifractal dimension distributions are easily observable comparing the different sea surface structures (fig. 9) and also in much smaller Reynolds number flows using laboratory experiments with LIF (Laser Induced Fluorescence) images of the evolution of a single jet (fig. 10) demonstrating that multifractal analysis can be used to distinguish among various turbulent structures both in environmental and laboratory flows.

Distinct fractal curves in both environmental cases are caused by the different conditions; free-jet–like structure is not limited by the coast existence like in wall-jet–like structure. In the case of experimental jet we have to take into account the 3 dimensionality of the flow (higher maximum value of the fractal dimension) and also factors like the range of scales or the different number of image pixels considered.

6. – Discussion and conclusions

The complex nature of velocity and scalar turbulent fields, both in fully developed turbulence and in non-homogeneous or non-equilibrium cascades has been studied under a self-similar approach since Richardson described the cascade process taking place in turbulent flows, and the equilibrium inertial sub-range in homogeneous turbulence was defined by Kolmogorov. Although Kolmogorov described also capacity as a measure equivalent to the box-counting fractal dimension [16, 17], that set the fractal methods and the different types of self-similar analysis.

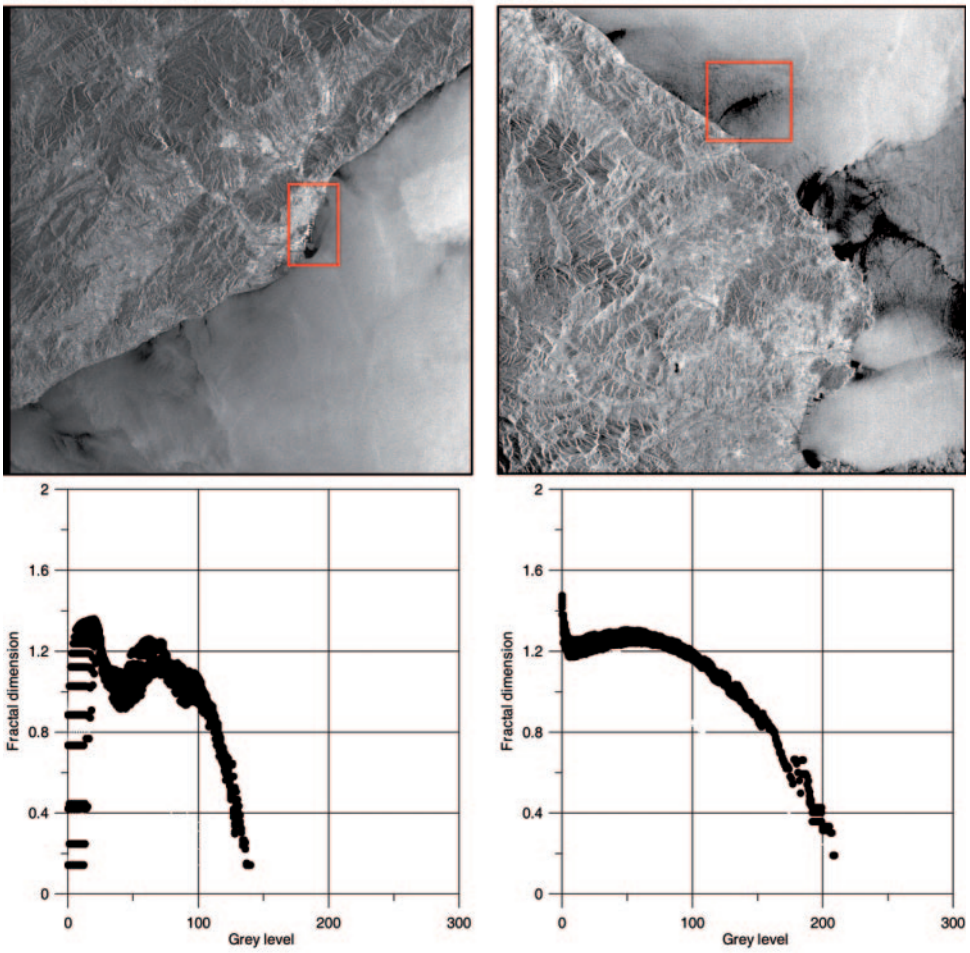

Fig. 9. – Examples of jets detected in the sea surface in the Gulf of Lion area (Barcelona—left and Girona—right). Differences between wall-jet–like (left) and free-jet–like (right) cases may be distinguished, as they show quite different multifractal plots (bottom).

We present here some examples of visualization methods applied to several laboratory experiments and in satellite images of jet-like flows and how image analysis is able to help in the study of the structure of the turbulence, if both velocity structure functions and multifractal measures can be compared both at the large (or external) scales, of the order of the integral length scale; and at the small (or internal) scales where mixing takes place, or the order of

$$\eta = \left(\frac{\nu^3}{\varepsilon}\right)^{1/4}, \tag{12}$$

which is the Kolmogorov scale, ν being the molecular viscosity and ε the local energy dissipation.

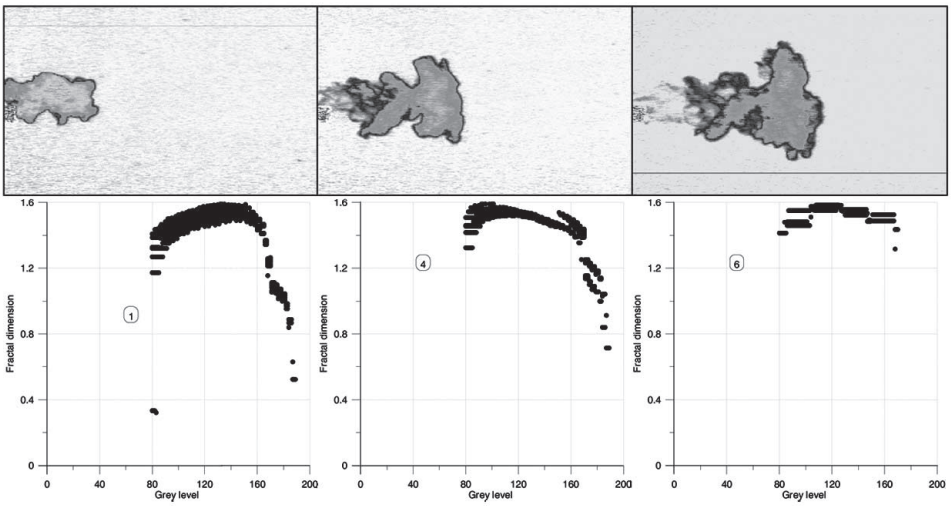

Fig. 10. – Examples of jet sequences (top) with their corresponding fractal dimension plots (bottom). Here the range of scales and intensity levels is smaller than in fig. 9.

We have investigated the structure of the ocean surface detected jets (SAR) and experimental configurations to compare wall and boundary effects on the structure of jets. From the definition of the structure function (10) the scaling with the length is

$$S_P(l) = c\varepsilon^{p/3} l^{p/3}, \tag{13}$$

but because there may be a dependence of the dissipation on the scale such as: $\langle \varepsilon_0 \rangle \, l^{\tau_p}$, it is interesting to relate the scaling exponent of the structure functions also to the fractal dimension following [11, 16, 18] with the standard notation, then we can separate the contribution of the scaling due to the dissipation from that of an inertial equilibrium cascade with no intermittency ($p/3$)

$$\xi_p = \frac{p}{3} + \tau_p. \tag{14}$$

Then it is easy to show that if the velocity has a scaling exponent (Holden) $h = 1/3 - [(3 - D)/3]$, D being the fractal dimension considered in the Beta model [16] that expresses the number of active eddies that remain from scale to scale (considering the situation of local equilibrium and homogeneity). This anomaly of the scaling of the structure functions is defined as intermittency, but instead of only considering the scaling of the dissipation, that leads to the definition of a single intermittency as

$$\mu = 2 - \xi_6, \tag{15}$$

we will use a generalized intermittency that may affect in a different way the different moments p.

$$\mu_p = 2\xi_{p/2} - \xi_p. \tag{16}$$

Using now the scaling of the dissipation, we can see that for 3D turbulence

$$\tau_P = \mu_p = (3 - D)\left(1 - \frac{p}{3}\right), \tag{17}$$

and then we can relate both the structure function and the spectral slope to the fractal dimension, which we will consider as the maximum of $D(\rho)$.

$$\xi_P = \frac{p}{3} + (3 - D)\left(1 - \frac{p}{3}\right), \tag{18}$$

$$E(k) = c\varepsilon_0 k^{-\left(5/3 + \frac{3-D}{3}\right)}. \tag{19}$$

Our aim is to investigate the turbulent and fractal structure of non-homogeneous jets and develop multifractal techniques useful for environmental monitoring in space as well as in the laboratory. We have confirmed that multifractal analysis can be used to distinguish among different turbulent structures. Wall jet behavior is used to compare spectral, structure function analysis with fractality using eqs. (18) and (19).

The role of dominant vortices, and specially those associated to boundary affects the multifractal plots, the cascade processes and the intermittency are related to the increase in r.m.s velocity fluctuations shown in fig. 6 (left)).

The series of experiments on three-dimensional velocity were measured with an ADV sonic velocimetry during long steady periods in order to improve the convergence of higher-order structure functions. The scale-to-scale transfer and the structure functions are calculated and from these the intermittency parameters. Some two point correlations and time lag calculations are used to investigate the time and spatial integral length scales obtained from both Lagrangian and Eulerian correlations and functions, and we compare these results with both the theoretical and experimental ones. The description of how to use structure functions to measure intermittency using the beta-model and the role of locality in higher-order exponents is described in [8-11]. In general it has to be remembered that the third-order structure function scaling exponent does not have to be one, in non-homogeneous or even in non-local flows, a compensation mechanism may act between the most energetic, but rare events or eddies and the common but weaker (and smaller) eddies [18, 19].

The results of the fractal analysis are only a geometrical tool but it is interesting to compare changes in the fractal dimension as an indication of the self-similarity transition to fully developed turbulence between the different experimental set-ups [20]. Information about the mixing can be extracted from the evolution of the fractal dimension measurements that can be now analyzed with a fast digitizer system ImaCalc.

It is apparent that the vorticity originated by the wall (or boundary layer) increases large-scale turbulence, and probably also mixing at the region of interaction between the jet and the vortices produced by it. This seems to occur both in the jets and plumes experiments indicating an increase in the maximum fractal dimension of the interface centre between $D_m = 1.3$ and 1.4. The spectral and fractal aspects of the field data are compared with the experiments, the relation between fractal analysis and spectral analysis can be very useful to determine the evolution of scales, even in the field with video recordings, or as presented here with SAR images [21, 22].

* * *

ES acknowledges a grant "Beca predoctoral UPC para investigacion" from Universitat Politecnica de Catalunya. The group of Turbulencia Fluctuacions i Diffusio (SGR99-00145) has provided some support for the research. Thanks are also due to Prof. Martinez Benjamin for help with the Satellite data. ESA-AO-CIP.2240 and ESP2005-07551.

REFERENCES

[1] Castilla Lopez R., *Simulación cinemática de flujo turbulento. Aplicación al estudio de la estructura de la turbulencia y de la difusión turbulenta*, Doctoral thesis, Universitat Politécnica de Catalunya (2001).
[2] Grau J., PhD Thesis. Univ. Politecnica de Catalunya, UPC, Teseo, Barcelona (2005).
[3] Redondo J. M. and Cantalapiedra I. R., *J. Flow Turbul. Combust.*, **51** (1993) 217.
[4] Castilla R., Redondo J. M., Gamez P. J. and Babiano A., *Non-Linear Processes Geophys.*, **14** (2007) 139.
[5] Redondo J. M., *Mixing efficiencies of different kinds of turbulent processes and instabilities, Applications to the environment*, in *Turbulent Mixing in Geophysical Flows*, edited by Linden P. F. and Redondo J. M. (CIMNE, Barcelona) 2001, pp. 131-157.
[6] Launder B. E. and Rodi W., *Annu. Rev. Fluid Mech.*, **15** (1983) 429.
[7] Kovasznay Leslie S. G., *Annu. Rev. Fluid Mech.*, **2** (1970) 95.
[8] Hinze J. O., *Turbulence*, 2nd edition (New York, McGraw-Hill) 1975.
[9] Rajaratnam N., *Turbulent Jets* (Elsevier, Amsterdam) 1976.
[10] Knowles K. and Myszko M., *Exp. Therm. Fluid Sci.*, **17** (1998) 71.
[11] Mahjoub O. B., *Non-local dynamics and intermittency in non-homogenous flows*, Doctoral thesis, Universitat Politecnica de Catalunya (2000).
[12] List E. J., *Annu. Rev. Fluid Mech.*, **14** (1982) 189.
[13] Van der Water W. and Herweijer J. A., *J. Fluid Mech.*, **387** (1999) 3.
[14] Voulgaris G. and Trowbridge J. H., *J. Atmos. Ocean. Technol.*, **15** (1997) 272.
[15] Mahjoub O. B., Redondo J. M. and Babiano A., *Appl. Sci. Res.*, **59** (1998) 299.
[16] Frish U., *Turbulence. The legacy of A. N. Kolmogorov* (Cambridge University Press) 1995.
[17] Kolmogorov A. N., *Proc. USSR Acad. Sci.*, **32** (1941) 16 (in Russian); *Proc. R. Soc. London, Ser. A*, **434** (1980) 15.
[18] Mahjoub O. B., Granata T. and Redondo J. M., *Phys. Chem. Earth B*, **26** (2001) 281.
[19] Redondo J. M., Grau J., Platonov A. and Garzón G., *Rev. Int. Mét. Num. Cálc. Diseño en Ing.*, **24** (2008) 25.
[20] Lane-Serff G. F., *J. Fluid Mech.*, **249** (1993) 521.
[21] Bezerra M. O., Diez M., Medeiros C., Rodriguez A., Bahia. E., Sanchez- Arcilla A. and Redondo J. M., *Appl. Sci. Res.*, **59** (1998) 191.
[22] Gade M. and Redondo J. M., *Marine pollution in European coastal waters monitored by the ERS-2 SAR: a comprehensive statistical analysis, IGARSS 99. Hamburg*, Vol. **2** (1999), pp. 1375-1377.